Carbon Market Price Forecasting in China Using Probability Density Recurrent Networks

Zijie Wei[1], Yongfei Hu[2], Pengyu Wang[3], Zhixin Han[4] and Qianjiao Xie[5, *]

12067684@ceic.com[1], 20069187@ceic.com[2], wangpy@whu.edu.cn[3], hanzhixin30@whu.edu.cn[4], xieqj1996@whu.edu.cn[5]

Longyuan(Beijing) Carbon Asset Management Technology Co., Ltd., Beijing, 100034, China[1, 2]
School of Economics and Management, Wuhan University, Wuhan, 430072, China[3, 4, 5]
Research Center for Complexity Science and Management, Wuhan University, Wuhan, 430072, China[3, 4, 5]

Abstract: With the nationwide proliferation of carbon markets, the scarcity of carbon emissions allowances has become comparable to other commodities in traditional markets, endowing them with unique market value. Carbon prices play a central role in carbon market mechanisms, reflecting the outcomes of market competition and shaping government policies related to carbon emissions allocation. Consequently, the accurate prediction of carbon prices is essential for businesses to comprehend fluctuations in carbon prices, efficiently manage carbon emissions, and provide a sound foundation for trading decisions. In this study, we address data uncertainty by developing a probability density recurrent network. We investigate the intricate interrelationships and evolving patterns among data points using probability density distribution functions in time series data, enabling the creation of a prediction model to anticipate future data points. Multiple evaluation criteria corroborate the precision and effectiveness of the methodology employed in this research.

Keywords: Time series; Probability density recurrent networks; Carbon price forecasting

1. Introduction

Establishing a nationwide carbon market has conferred upon carbon emission allowances a scarcity akin to other market commodities, thus endowing them with unique market value. Henceforth, the pivotal significance of carbon prices unfolds within the mechanisms of the carbon market. They not only mirror the outcomes of market competition but also act as a directive signal guiding the allocation of government carbon emissions. Understanding the dynamics of carbon prices, their driving factors, and precise forecasting are paramount, as they directly influence carbon price predictions. Accurate carbon price forecasting aids carbon reduction enterprises in gaining a thorough comprehension of and managing the patterns of carbon price fluctuations, effectively handling the associated revenue and risks, and providing a scientific basis for trading decisions.

In the past, carbon price research predominantly relied on univariate and multivariate linear models, but these approaches proved flawed. For instance, Daskalakis et al. observed that spot prices of carbon emission allowances in the European Union Emissions Trading Scheme (EU ETS) exhibited a random walk pattern, which could be captured through jump-diffusion

PMBDA 2023, December 15-17, Nanjing, People's Republic of China

DOI 10.4108/eai.15-12-2023.2345396

models[1]. Paolella and Taschini found that EU carbon allowance prices could be effectively modeled by a generalized asymmetric t-distribution GARCH model[2]. Seifert et al. noted time-dependent volatility structures in EU carbon prices[3], and Benz and Trück replicated the nonlinear dynamics of EU carbon prices through Markov switching models[4]. In general, carbon prices exhibit nonlinearity, instability, leverage effects, asymmetry, and regional heterogeneity, influenced by factors like trading systems, environmental heterogeneity, and related policies, resulting in nonlinear, nonstationary, and multi-frequency characteristics in regional carbon emission trading prices[5–7].

Various methods have been employed in carbon price forecasting, with earlier research relying on qualitative analysis. Current research utilizes more sophisticated approaches, mainly categorized into three major classes: statistical and econometric methods, artificial intelligence methods, and hybrid forecasting methods. For instance, Chevallier utilized non-parametric techniques in carbon price forecasting, achieving a nearly 15% reduction in prediction errors compared to conventional linear autoregressive models[8]. Byun and Cho conducted an analysis using data from the European Futures Exchange and determined that, in specific scenarios, GJR-GARCH models outperformed TGARCH and GARCH models[9]. Koop and Tole applied dynamic model averaging in their endeavor to predict carbon prices, introducing three distinct advantages compared to conventional approaches. Initially, it facilitated the dynamic adjustment of coefficients for predictive variables over time. Additionally, it allowed for the continuous evolution of the entire forecasting model. Finally, it overcame statistical issues arising from numerous potential predictive factors explaining carbon prices.[10]. Drawing upon EU carbon emission price data, Eugenia Sanin et al. employed ARMAX-GARCH models, incorporating dynamic jump probabilities, to predict carbon prices. Their method surpassed the forecasting accuracy of standard ARMAX-GARCH models in capturing the intricacies of carbon price dynamics.[11]. Despite these models performing high prediction accuracy based on stationary data and linear assumptions, they fall short in efficiently handling the nonlinearity of carbon price fluctuations.

As artificial intelligence progresses swiftly, innovative approaches have emerged to address the constraints inherent in statistical and econometric models. These solutions have been successfully introduced and applied across diverse forecasting domains, such as in the realm of wind energy forecasting. For example, Zhu et al. developed an adaptive multi-scale ensemble learning paradigm combining ensemble empirical mode decomposition (EEMD), particle swarm optimization, and least squares support vector machines with kernel prototype, significantly improving carbon price prediction accuracy compared to popular forecasting methods, demonstrating high accuracy in both magnitude and orientation forecasts[12]. Xu et al. introduced an innovative approach to predict carbon prices by leveraging time series complex network analysis techniques in conjunction with the extreme learning machine. By conducting empirical assessments with carbon emission price data across the second, third, and transitional stages of the EU ETS, the CPN-ELM model emerged as an effective enhancer of forecasting precision. This was particularly evident in its improved accuracy in predicting both the magnitude and directionality of carbon prices[13]. In contrast to statistical and econometric approaches, artificial intelligence methods demonstrate heightened predictive efficacy owing to their remarkable modeling prowess in capturing nonlinear shifts in carbon prices. However, due to inherent limitations, single models cannot consistently attain the desired performance.

Moreover, considering the significant volatility of carbon prices, the performance of artificial intelligence methods is not always ideal.

To further enhance predictive capabilities and harness diverse methodologies, hybrid forecasting approaches have gained prominence across various research domains and applications. In the realm of carbon price forecasting, modern hybrid models primarily utilize methods such as data decomposition, optimization algorithms, and various forecasting models. These models amalgamate the strengths of different methodologies to attain accurate predictions of carbon prices. For instance, Zhou et al. formulated a pioneering hybrid framework to predict carbon prices, amalgamating extreme symmetry mode decomposition, ELM, and grey wolf optimization techniques[7]. Zhang et al. proposed a hybrid model that combines complete EEMD, cointegration models, generalized autoregressive conditional heteroskedasticity models, GARCH, and ant colony optimization for grey neural network. This approach demonstrated superior performance compared to other models, as evidenced by data from the EU ETS[14]. Sun and Huang presented a novel hybrid model for forecasting carbon prices. This model integrates secondary decomposition algorithms originating from both empirical mode decomposition and variational mode decomposition, incorporates genetic algorithms and backpropagation neural networks, offering an innovative perspective on carbon price prediction[15].

2. Analysis of Carbon Market Characteristics

The nationwide unified carbon market commenced official trading on July 16, 2021. The initial carbon compliance period encompassed 2,162 crucial emission units within the power generation sector, accounting for an annual greenhouse gas emission coverage of approximately 4.5 billion tons of carbon dioxide. As of September 28, 2023, the national carbon market has been operational for a cumulative 538 trading days, with a total traded volume of 254 million tons of carbon emission allowances and a cumulative transaction value of ¥11.903 billion. Among these, the listed agreement transactions have accumulated a traded volume of 41.3298 million tons and a total transaction value of ¥2.076 billion. In comparison, the bulk agreement transactions have reached a cumulative traded volume of 212.7623 million tons and a total transaction value of ¥9.827 billion.

Concerning the total traded volume and transaction value, both exhibit an inverted "V" shaped trend, characterized by an initial increase followed by a decrease, as shown in **Figure 1**. Both reached their highest values in December 2021 and their lowest in September 2022. Similarly, the traded volume and transaction value of the listed and bulk agreements followed the same trends, showing a peak at the end of 2021 and a low point in August 2022.

Regarding carbon quota price trends, the national carbon price has undergone a process of initial suppression followed by an upturn, gradually stabilizing. The CEA price has remained around ¥60 per ton. On December 31, 2021, the closing price was ¥54.22 per ton, marking a 12.96% increase from the opening price on July 16. The first carbon compliance period concluded successfully, with a compliance rate of 99.5% based on the carbon compliance volume. Over half of the critical emission units actively participated in market trading, contributing to a stable increase in market transaction prices.

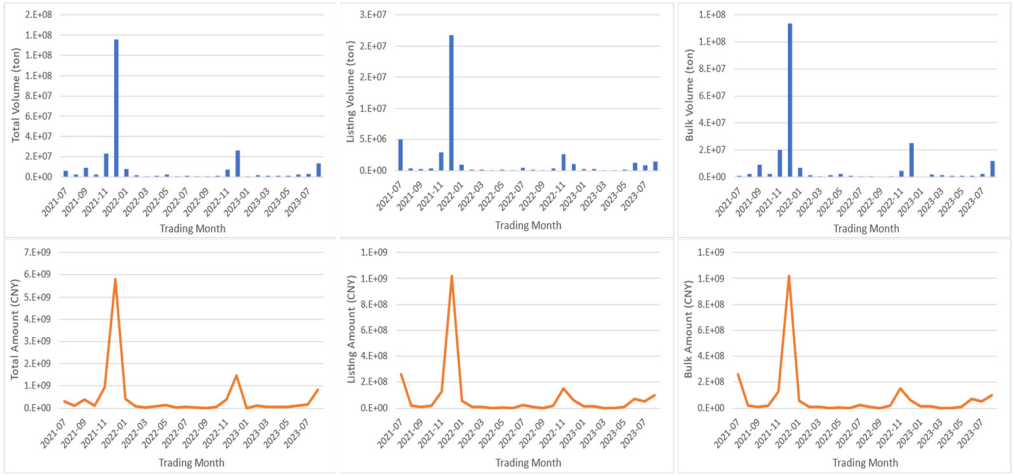

(a) Monthly Total Trading Value (b) Monthly Listed Agreement Trading Value (c) Monthly Bulk Agreement Trading Value

Figure 1. Monthly Carbon Market Trading Volume and Transaction Value.

In national carbon trading from July 2021 to August 2023, concerning monthly carbon prices, there is a clear V-shaped trend, initially declining and then rising. The difference between the highest and lowest monthly carbon prices has gradually decreased, as illustrated in **Figure 2**. The lowest monthly price was recorded in October 2021 at ¥38.5 per ton, while the highest was observed in August 2023 at ¥62.6 per ton. The highest monthly price was at its lowest in November 2021, at ¥46 per ton, and peaked in August 2023 at ¥75 per ton. The most significant price gap between the highest and lowest monthly prices occurred in December 2021, with a difference of ¥22.29 per ton. In contrast, in November 2022, the highest and lowest monthly prices were closest, with a difference of only ¥0.9 per ton.

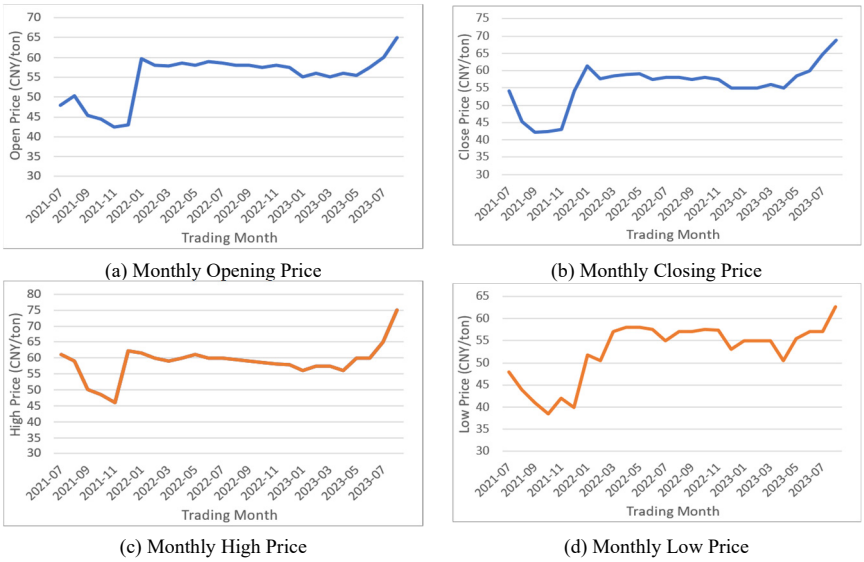

(a) Monthly Opening Price (b) Monthly Closing Price

(c) Monthly High Price (d) Monthly Low Price

Figure 2. Monthly Carbon Market Prices.

3. Carbon Price Forecasting Methods

Anticipating fluctuations in the carbon market and prices requires a thorough examination of data uncertainty. Initially, we estimate a series of the probability density distribution function (PDF) based on time-series data. Each PDF, associated with a specific time point, is treated as a node in the network. Following this, a Recursive Network of Probability Densities (RNPD) is established, utilizing the topological structure and applying link prediction theory to assess the similarity between nodes. This method enables a thorough exploration of the connection relationships and developmental trends among these nodes, facilitating the construction of prediction models for anticipating future nodes.

3.1. Construction of PRDN

Consider the observable variables x_i and x_j correspond to random variables $X_i$and X_j at times i and j, and define $D_{ij} = X_i - X_j$ as the difference between variables x_i and x_j. The probability of repetitions below a threshold ε can be expressed as equation (1).

$$P_{ij}(\varepsilon) := \mathrm{Prob}\big(|D_{ij}| \le \varepsilon\big). \tag{1}$$

This can be computed by equation (2).

$$P_{ij}(\varepsilon) = \int_{-\infty}^{+\infty} \rho_i^X(x_i) \int_{x_i-\varepsilon}^{x_i+\varepsilon} \rho_{ji|i}^X\big(x_j \mid x_i\big) dx_i dx_j = \int_{-\infty}^{+\infty} \int_{x_i-\varepsilon}^{x_i+\varepsilon} \rho_{ij}^X\big(x_i, x_j\big) dx_i dx_j . \tag{2}$$

where $\rho_{ij}^X\big(x_i, x_j\big)$ represents the joint probability density. By relating the density functions to the distribution functions, the recursive probability $P_{ij}(\varepsilon)$ can be interpreted as the total probability of $D_{ij} = X_i - X_j$ within the interval $[-\varepsilon, \varepsilon]$. Thus, the equation can be rewritten as equation (3).

$$P_{ij}(\varepsilon) = \mathrm{Prob}\left(|D_{ij}| \le \varepsilon\right) = \mathrm{Prob}\left(D_{ij} \le \varepsilon\right) - \mathrm{Prob}\left(D_{ij} \le -\varepsilon\right). \tag{3}$$

Which implies equation (4).

$$P_{ij}(\varepsilon) = F_{ij}^D(\varepsilon) - F_{ij}^D(-\varepsilon). \tag{4}$$

where $F_{ij}^D\big(d_{ij}\big) := \mathrm{Prob}\left(|D_{ij}| \le d_{ij}\right)$, and $d_{ij} \in (-\infty, +\infty)$ is the cumulative distribution function (CDF) of D_{ij}.

The upper limit $M_{ij}$and lower limit m_{ij} of the CDF $F_{ij}^D\big(d_{ij}\big)$ can be estimated by equation (5)

$$\begin{cases} M_{ij}\big(d_{ij}\big) = \min\left\{\inf_{\tau} f_{ij}\big(\tau, d_{ij}\big), 0\right\} + 1 \\ m_{ij}\big(d_{ij}\big) = \max\left\{\sup_{\tau} f_{ij}\big(\tau, d_{ij}\big), 0\right\} \end{cases}. \tag{5}$$

where $f_{ij}\big(\tau, d_{ij}\big) = F_i^X(\tau) - F_j^X\big(\tau - d_{ij}\big)$.

For all $D_{ij} = d_{ij}$, it holds that $F_{ij}^D\big(d_{ij}\big) \in \big[m_{ij}\big(d_{ij}\big), M_{ij}\big(d_{ij}\big)\big] \subseteq [0,1]$. The upper bound $P_{ij}^u(\varepsilon)$ and lower bound $P_{ij}^l(\varepsilon)$ of the recursive probability $P_{ij}(\varepsilon)$ can be expressed as equation (6).

$$\begin{cases} P_{ij}^u(\varepsilon) = \min\big\{M_{ij}(\varepsilon) - m_{ij}(-\varepsilon), 1\big\} \\ P_{ij}^l(\varepsilon) = \max\big\{m_{ij}(\varepsilon) - M_{ij}(-\varepsilon), 0\big\} \end{cases}. \tag{6}$$

With the recursive threshold ε established, it is ensured that $P_{ij}(\varepsilon) \in \left[P_{ij}^{l}(\varepsilon), P_{ij}^{u}(\varepsilon)\right] \subseteq [0,1]$. Assuming the probability $P_{ij}(\varepsilon)$ is a random variable distributed within the interval $\left[P_{ij}^{l}(\varepsilon), P_{ij}^{u}(\varepsilon)\right]$, its probability density is denoted as $\rho_{ij}^{P}(p_{ij})$. Consequently, the connection probability between sequences at times i and j is expressed as equation (7).

$$\mathrm{Prob}\left(A_{ij}=1\right)=\int_{P_{ij}^{l}}^{P_{ij}^{u}}\rho_{ij}^{A|P}\left(A_{ij}=1 \mid p_{ij}\right)\rho_{ij}^{P}(p_{ij})dp_{ij}=\int_{P_{ij}^{l}}^{P_{ij}^{u}}p_{ij}^{u}\rho_{ij}^{P}(p_{ij})dp_{ij}=E_{\rho_{ij}^{P}}\left[P_{ij}\right]. \quad (7)$$

where $\rho_{ij}^{A|P}\left(A_{ij}=1 \mid p_{ij}\right)$ represents the probability of $A_{ij}=1$ given $P_{ij}=p_{ij}$. The result from the above equation shows that the expected value of the utility random variable P_{ij} can be calculated to determine the probability of connections between nodes. Assuming P_{ij} follows a uniform distribution within the range $\left[P_{ij}^{l}, P_{ij}^{u}\right]$, the overall probability at i and j is equation (8).

$$\mathrm{Prob}\left(A_{ij}=1\right)=E_{\rho_{ij}^{p}}\left[P_{ij}\right]=\left(P_{ij}^{l}+P_{ij}^{u}\right)/2. \quad (8)$$

In summary, the adjacency matrix of PDRN is constructed as follows equation (9).

$$\hat{A}_{ij}(\varepsilon)=\begin{cases}\left(P_{ij}^{l}(\varepsilon)+P_{ij}^{u}(\varepsilon)\right)/2, i\neq j\\ 0, i=j\end{cases}. \quad (9)$$

The presented equation elucidates that the entries within the adjacency matrix range between [0,1], signifying the probabilities of connections among network nodes. PDRN operates as a weighted network, with connection probabilities serving as weights. Leveraging the topological structure of the network provides a lucid depiction of potential connections and their respective strengths among nodes. Furthermore, given that PDRN is constructed based on PDFs derived from the original data, it not only encapsulates numerical information from the source data but also accommodates inherent data uncertainty. Consequently, employing the topological structure of PDRN for the analysis of original data emerges as an effective approach for uncertainty analysis.

3.2. Determining Node Similarity Using Link Prediction

The Link Prediction approach employing Local Random Walk (LRW) can be applied to identify prospective edges within the network. The random walk states of network nodes are encapsulated in a probability transition matrix denoted as P. Within a weighted network consisting of N nodes, the computation of the transition probability from node i to node j is expressed by equation (10).

$$P_{ij}=w_{ij}/s_i. \quad (10)$$

where w_{ij} is the probability of a connection between nodes i and j, with $0<w_{ij}\leq 1$ if nodes i and j are connected; otherwise $w_{ij}=0$. The strength of node i, denoted as s_i, is defined as $s_i=\sum_j w_{ij}$. After t steps, $\overrightarrow{\pi_i}$ is given by equation (11).

$$\overrightarrow{\pi_i}(t)=P^T\overrightarrow{\pi_i}(t-1). \quad (11)$$

where, $\overrightarrow{\pi_i}$ is the probability of moving from node i to other nodes, P^T signifies the transpose of matrix P. At the initial state $t=0$, $\overrightarrow{\pi_i}(0)$ represents the random walkers located at node i, with dimensions $N\times 1$. The i-th element of $\overrightarrow{\pi_i}(0)$ equals 1, while all other elements are set to 0.

Assuming the initial resource distribution for each node is $s_i/(2|E|)$, where $|E|$ represents the number of network edge connections, the similarity between node i and j after each step can be computed as equation (12).

$$S_{ij}^{LRW}(t) = \frac{s_i}{2|E|}\pi_{ij}(t) + \frac{s_i}{2|E|}\pi_{ji}(t). \tag{12}$$

However, during the drift from node i to j, even when nodes i and j are very close, the walker may gradually move away from both nodes. In this case, due to the tendency of walkers to stay in the local area rather than drift to the rest of the network, the prediction accuracy may be reduced. Therefore, by superimposing the random walk processes of each step, the resultant similarity between nodes is ultimately heightened, as depicted in (13).

$$S_{ij}^{SRW}(t) = \sum_{l=1}^{t} S_{ij}^{LRW}(l). \tag{13}$$

where, SRW represents Superimposed Random Walk.

In summary, the equation above is used to calculate the similarity between node N and the previous $N-1$ nodes, denoted as $S^{SRW} = \left[S_{1N}, S_{2N}, \cdots, S_{(N-1)N}\right]$. The results are sorted in descending order, $S_{M(1)N}, S_{M(2)N}, \cdots, S_{M(N-1)N}$, corresponding to nodes $\left(t_{M(1)}, y_{M(1)}\right), \left(t_{M(2)}, y_{M(2)}\right), \cdots, \left(t_{M(k)}, y_{M(k)}\right)$, which are the top k nodes most similar to the last node (t_N, y_N).

3.3. Construction of Prediction Models

Weighted Prediction Method Based on Similar Node Trend. To predict node (t_{N+1}, y_{N+1}), which is the next point after node (t_N, y_N) and the closest point to it, the trend of change from (t_N, y_N) to (t_{N+1}, y_{N+1}) is assumed to be similar to the trends of change from $\left(t_{M(1)}, y_{M(1)}\right), \left(t_{M(2)}, y_{M(2)}\right), \cdots, \left(t_{M(k)}, y_{M(k)}\right)$ to their respective next nodes. Hence, the method put forward employs the weighted amalgamation of the shift pattern from the top k nodes exhibiting high similarity to the node (t_N, y_N) for forecasting the shift in the pattern of the present state. The prediction equation is as follows equation (14).

$$y_{N+1} = \sum_{i=1}^{k} \alpha_i \frac{y_{M_{(i)}+1} - y_{M_{(i)}}}{t_{M_{(i)}+1} - t_{M_{(i)}}}(t_{N+1} - t_N) + y_N. \tag{14}$$

where $\alpha_i = S_{M_{(i)}\mathrm{N}} / \left(\sum_{i=1}^{k} S_{M_{(i)}\mathrm{N}}\right)$ represents the weights.

The setup process of this prediction model demonstrates its utilization of PDRN and link prediction approaches alongside the original dataset. This allows for the recognition of numerous historical states resembling the current one. Following this, the model utilizes the weighted developmental patterns extracted from these historical states to predict changes in the current state's trends. For instance, when unforeseen events lead to fluctuations in carbon prices, the model incorporates the impacts of similar historical events on changes in carbon prices to generate predictions.

Weighted Prediction Method for Extrapolation of Similar Node Trends. In contrast to the previous prediction, after obtaining the top k nodes highly similar to node (t_N, y_N), the model carries out a weighted projection of the connection patterns between these similar nodes and the last node to predict future nodes. The prediction model is as follows equation (15).

$$y_{N+1} = \sum_{i=1}^{k} \alpha_i \frac{y_N - y_{M_{(i)}}}{t_N - t_{M_{(i)}}}\left(t_{N+1} - t_{M_{(i)}}\right) + y_N. \tag{15}$$

This prediction model focuses on the continuity of changes in the prediction target, where future states are expected to continue from past and current states, for example, the continuous upward or downward fluctuations in carbon trading prices.

3.4. Combined Prediction

The two aforementioned prediction models are characterized by distinct focal points. Carbon price variations can be broadly classified into two categories: those exhibiting a sustained and continuous trend, amenable to prediction by the first model, and those experiencing abrupt and irregular shifts, suitable for prediction using the second model. To amalgamate the strengths of these two models, accommodating the forecasting of both abrupt and continuous price changes, a unified prediction model is formulated through the following steps:

(1) Define Node Distances: The distances between node $\left(t_{M(i)}, y_{M(i)}\right)$ and node (t_N, y_N), node $\left(t_{M(i)}, y_{M(i)}\right)$ and node (t_{N+1}, y_{N+1}), and node (t_N, y_N) and node (t_{N+1}, y_{N+1}) are determined using the equations (16)–(18).

$$d_{M_{(i)}\to N} = t_N - t_{M_{(i)}}. \tag{16}$$

$$d_{M_{(i)}\to N+1} = t_{N+1} - t_{M_{(i)}}. \tag{17}$$

$$d_{N\to N+1} = t_{N+1} - t_N. \tag{18}$$

(2) Determine Weight Coefficients: When the separation between node $\left(t_{M(i)}, y_{M(i)}\right)$ and node (t_{N+1}, y_{N+1}) is considerable (indicated by a large value of $d_{M_{(i)}\to N}$), the likeness between nodes within the network will diminish. In this scenario, weights are assigned according to the distance between nodes to measure similarity. The weight coefficients are defined as follows equations (19)~(20).

$$w_1 = d_{N\to N+1} / \left(\sum_{i=1}^{k} d_{M_{(i)}\to N+1}\right). \tag{19}$$

$$w_2 = \sum_{i=1}^{k} d_{M_{(i)}\to N} / \left(\sum_{i=1}^{k} d_{M_{(i)}\to N+1}\right). \tag{20}$$

where w_1 is the weight coefficient for the Similar Node Trend Change Weighted Prediction Method, and w_2 is the weight coefficient for the Weighted Prediction Method for Extrapolation of Similar Node Trends.

(3) Combined Prediction: Assuming that the results obtained from the first method are represented as Y_1, and the results from the second method are represented as Y_2, the final prediction is given by equation (21).

$$\hat{y}_{N+1} = w_1 Y_1 + w_2 Y_2 \tag{21}$$

Thus, the combined prediction model for predicting (t_{N+1}, y_{N+1}) based on the top k similar nodes is expressed as equation (22).

$$\hat{y}_{N+1} = w_1 \left(\sum_{i=1}^{k} \alpha_i \frac{y_{M_{(i)+1}} - y_{M_{(i)}}}{t_{M_{(i)+1}} - t_{M_{(i)}}} (t_{N+1} - t_N) + y_N\right) + w_2 \left(\sum_{i=1}^{k} \alpha_i \frac{y_N - y_{M_{(i)}}}{t_N - t_{M_{(i)}}} \left(t_{N+1} - t_{M_{(i)}}\right) + y_N\right) \tag{22}$$

(4) Prediction Accuracy: To evaluate the prediction performance, four accuracy measurement metrics are calculated as follows equations (23)~(26).

$$MAE = \frac{1}{N} \sum_{t=1}^{N} |\hat{y}_t - y_t| \tag{23}$$

$$MAPE = \frac{1}{N} \sum_{t=1}^{N} \left|\frac{\hat{y}_t - y_t}{y_t}\right| \tag{24}$$

$$SMAPE = \frac{1}{N}\sum_{t=1}^{N}\frac{|\hat{y}_t - y_t|}{\hat{y}_t + y_t} \quad (25)$$

$$RMSE = \sqrt{\frac{1}{N}\sum_{t=1}^{N}(\hat{y}_t - y_t)^2} \quad (26)$$

4. Carbon Price Forecasting Results

Since the establishment of the national carbon market in China in July 2021, the carbon market has undergone a period of development, and there is now data on carbon prices for over 500 days. The data used for carbon prices in this study consists of daily maximum and minimum prices from the national carbon market, spanning from July 16, 2021, to September 28, 2023. The data was sourced from the carbon neutrality section of the CSMAR database, comprising a total of 538 sample data points, as depicted in **Figure 3**.

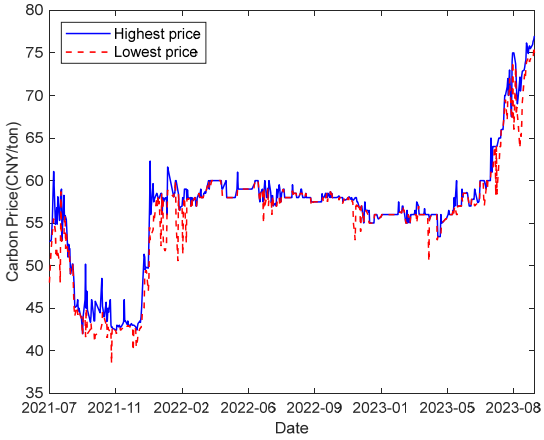

Figure 3. Carbon Price Trends from July 16, 2021, to September 28, 2023.

As **Figure 3** illustrates, carbon trading prices have exhibited significant fluctuations without a clear pattern. Since establishing the national carbon market (from July 16, 2021, to September 28, 2023), carbon prices have fluctuated between 38.5 CNY per ton to 77 CNY per ton. In the early stages, these fluctuations were quite pronounced, signifying a high degree of instability in the carbon market. Despite a subsequent increase in carbon prices over time, noticeable volatility persisted. Consequently, accurately predicting carbon prices and their changing trends is paramount.

To evaluate the predictive accuracy of carbon prices using data from the national carbon market since its establishment (from July 16, 2021, to September 28, 2023), we performed a forecasting analysis. In the beginning, we employed carbon pricing information spanning from July 16, 2021, to April 30, 2023, as the training set for forecasting the carbon price on May 1, 2023. Subsequently, we integrated the observed carbon price on May 1, 2023, into the prediction model for estimating the price on May 2, 2023. This process was repeated until we obtained the carbon price forecast results for September 28, 2023, as shown in **Figure 4 and Figure 5**.

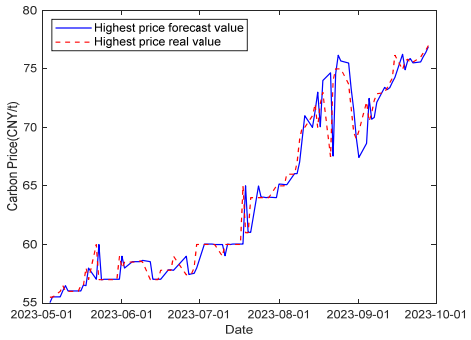

Figure 4. Forecast of Daily Maximum Carbon Prices from September 1, 2022, to November 28, 2022.

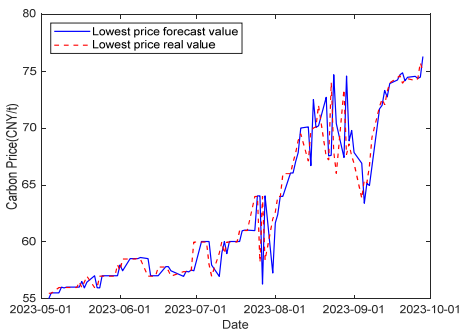

Figure 5. Forecast of Daily Minimum Carbon Prices from May 1, 2023, to September 28, 2023.

To assess the accuracy of the predictions made for daily maximum and minimum carbon prices from May 1, 2023, to September 28, 2023, the results were compared to the actual values, as presented in **Table 1**.

Table 1. Forecast Accuracy for Daily Maximum and Minimum Carbon Prices.

Accuracy Metric	MAE	MAPE	SMAPE	RMSE
Daily Maximum Carbon Price	0.8798	0.0133	0.0067	1.5507
Daily Minimum Carbon Price	1.2006	0.0185	0.0092	2.1372

From **Table 1**, it is evident that, based on four different error measurement methods, the errors between the predicted and actual values for daily maximum and minimum carbon prices from May 1, 2023, to September 28, 2023, are relatively small. Among these metrics, the symmetric mean absolute percentage error exhibits the least magnitude, followed by the mean absolute percentage error, while the root mean square error records the greatest numerical value. Hence, using carbon price data from July 16, 2021, to September 28, 2023, we have generated forecasts for the carbon prices over the next 20 days, as presented in **Table 2**.

Table 2. Forecast of Carbon Prices for the Next 20 Days.

Date	Daily Maximum Carbon Price	Daily Minimum Carbon Price	Date	Daily Maximum Carbon Price	Daily Minimum Carbon Price
Day 1	77.35	75.27	Day 11	80.46	80.18
Day 2	77.69	75.53	Day 12	80.51	80.24
Day 3	78.00	76.04	Day 13	80.56	80.31
Day 4	78.31	76.56	Day 14	80.61	80.38
Day 5	78.61	77.08	Day 15	80.67	80.44
Day 6	78.92	77.59	Day 16	80.72	80.51
Day 7	79.23	78.11	Day 17	80.77	80.57
Day 8	79.54	78.63	Day 18	80.82	80.64
Day 9	79.85	79.14	Day 19	80.87	80.71
Day 10	80.15	79.66	Day 20	80.92	80.77

5. Conclusion

In summary, since establishing the national carbon market, carbon trading prices have exhibited significant fluctuations and instability. Using time series data and constructing a PDRN for prediction, we conducted carbon price forecasts from May 1, 2023, to September 28, 2023. Our predictive model demonstrated exemplary performance in forecasting daily maximum and minimum carbon prices, with minor errors, particularly the symmetric mean absolute percentage error being the smallest and the root mean square error being the largest.

In conclusion, despite significant fluctuations in carbon prices, our predictive model exhibited reasonable accuracy in carbon price forecasting. These forecast results can support businesses and government decision-making in the carbon market, helping manage the costs and risks associated with carbon emissions and better adapt to the volatility and instability of the carbon emission market. However, it is essential to closely monitor market changes and policy adjustments and continuously improve and update predictive models to adapt to the dynamic nature of the carbon market.

Acknowledgments. This research was financially supported the National Social Science Fund of China (Grant No. 19ZDA083) and National Energy Group Investment Project LYH-2021-016.

References

[1] Daskalakis G., Psychoyios D., Markellos R. N.: Modeling CO2 emission allowance prices and derivatives: Evidence from the European trading scheme. Journal of Banking & Finance. Vol. 33(7), pp. 1230-1241. (2009)

[2] Paolella M. S., Taschini L.: An econometric analysis of emission allowance prices. Journal of Banking & Finance. Vol. 32(10), pp. 2022-2032. (2008)

[3] Seifert J.: Uhrig-Homburg M, Wagner M. Dynamic behavior of CO2 spot prices. Journal of Environmental Economics and Management. Vol. 56(2), pp. 180-194. (2008)

[4] Benz E., Trück S.: Modeling the price dynamics of CO2 emission allowances. Energy Economics. Vol. 31(1), pp. 4-15. (2009)

[5] Han M., Ding L., Zhao X., et al.: Forecasting carbon prices in the Shenzhen market, China: The role of mixed-frequency factors. Energy. Vol. 171, pp. 69-76. (2019)

[6] Liu X., Jin Z.: An analysis of the interactions between electricity, fossil fuel and carbon market prices in Guangdong, China. Energy for Sustainable Development. Vol. 55, pp. 82-94. (2020)

[7] Zhou J., Huo X., Xu X., et al. Forecasting the Carbon Price Using Extreme-Point Symmetric Mode Decomposition and Extreme Learning Machine Optimized by the Grey Wolf Optimizer Algorithm. Energies. Vol. 12(5), pp. 950. (2019)

[8] Chevallier J.: Nonparametric modeling of carbon prices. Energy Economics. Vol 33(6), pp. 1267-1282. (2011)

[9] Byun S. J., Cho H.: Forecasting carbon futures volatility using GARCH models with energy volatilities. Energy Economics. Vol. 40, pp. 207-221. (2013)

[10] Koop G., Tole L.: Forecasting the European Carbon Market. Journal of the Royal Statistical Society Series A: Statistics in Society. Vol. 176(3), pp. 723-741. (2013)

[11] Eugenia Sanin M., Violante F., Mansanet-Bataller M.: Understanding volatility dynamics in the EU-ETS market. Energy Policy. Vol. 82, pp. 321-331. (2015)
[12] Zhu B., Shi X., Chevallier J., et al.: An Adaptive Multiscale Ensemble Learning Paradigm for Nonstationary and Nonlinear Energy Price Time Series Forecasting. Journal of Forecasting. Vol. 35(7), pp. 633-651. (2016)
[13] Xu H., Wang M., Jiang S., et al.: Carbon price forecasting with complex network and extreme learning machine. Physica A: Statistical Mechanics and its Applications. Vol 545, pp. 122830. (2020)
[14] Zhang J., Li D., Hao Y., et al.: A hybrid model using signal processing technology, econometric models and neural network for carbon spot price forecasting Journal of Cleaner Production. Vol. 204, pp. 958-964. (2018)
[15] Sun W., Huang C.: A carbon price prediction model based on secondary decomposition algorithm and optimized back propagation neural network. Journal of Cleaner Production. Vol. 243, pp. 18671. (2020)